J|A|C|S
ARTICLES
Published on Web 06/21/2002

Late First-Row Transition-Metal Complexes of Texaphyrin

Sharon Hannah,[‡] Vincent Lynch,[‡] Dirk M. Guldi,[†] Nikolay Gerasimchuk,[⊥] Charles L. B. MacDonald,[§] Darren Magda,*[,⊥] and Jonathan L. Sessler[‡,*]

Contribution from the Department of Chemistry and Biochemistry, University of Texas at Austin, Austin, Texas 78712, Radiation Laboratory, University of Notre Dame, Notre Dame, Indiana 46556, Department of Chemistry and Biochemistry, University of Windsor, Windsor, Ontario N9B 3P4, Canada, and Pharmacyclics, Inc., 995 East Arques Avenue, Sunnyvale, California 94085

Received December 21, 2001

Abstract: The preparation of first-row transition-metal complexes of texaphyrin, a porphyrin-like, monoanionic penta-aza macrocyclic ligand, is reported. Specifically, the synthesis of organic-soluble Mn(II) (**1**), Co(II) (**2**), Ni(II) (**3**), Zn(II) (**4**), and Fe(III) (**5**) texaphyrin derivatives and their water-soluble counterparts (**6**−**10**) from appropriate metal-free, nonaromatic macrocyclic precursors is described. It was found that metal cations of sufficient reduction potential could act to oxidize the nonaromatic macrocyclic precursor in the course of metal insertion. Complexes were characterized by X-ray diffraction analysis, electrochemistry, flash photolysis, and EPR spectroscopy. The structural and electronic properties of these "expanded porphyrin" complexes are compared with those of analogous porphyrins. Notably, the texaphyrin ligand is found to support the complexation of cations in a lower valence and a higher spin state than do porphyrins. Interactions between the coordinated cation and the ligand π system appear to contribute to the overall bonding. Texaphyrin complexes of Mn(II), Co(II), and Fe(III) in particular may possess sufficient aqueous stability to permit their use in pharmaceutical applications.

Introduction

Texaphyrin is a penta-aza porphyrin-like macrocycle that has found utility as a ligand for large metal cations, particularly those of the trivalent lanthanide series.[1] Highly stable coordination complexes have been prepared not only with lanthanide(III) cations but also with yttrium(III), indium(III), and cadmium(II) salts.[2] Currently, the gadolinium(III) and lutetium(III) texaphyrin complexes (Gd-Tex, motexafin gadolinium; Lu-Tex, motexafin lutetium), in water-soluble form (Tex_c), are undergoing clinical testing as adjuvants for X-ray radiation therapy and photodynamic therapy, respectively.[3]

Recent photophysical and electrochemical studies of lanthanide(III) texaphyrin complexes have led to an appreciation that these properties show some dependence on the identity of the metal cation.[2,4] The incorporation of metal cations with a greater range in charge, size, and redox activity should result in a larger variance in these properties. This, in turn, provides an incentive to make and study texaphyrin-based transition metal complexes. Recently, we reported the synthesis and structure of a Mn(II) texaphyrin ($Mn\text{-}Tex_a^+$).[5] This complex, again in water-soluble form ($Mn\text{-}Tex_c^+$), was found to catalyze the disproportionation of peroxynitrite, a reactive oxygen species implicated in numerous clinical disorders, including atherosclerosis, ALS, and cancer.[6] The possibility of finding new complexes with beneficial biological properties provides an added incentive to develop the transition-metal chemistry of texaphyrins.

Much of the interest in the texaphyrin ligand stems from its structural resemblance to porphyrins. While its transition metal chemistry has not hitherto been extensively explored, that of the porphyrins is highly developed. In fact, porphyrin complexes derived from nearly every transition metal are known. Most of these complexes are very stable. However, in some cases, the cations in question are too large to sit within the porphyrin core, thus forming less stable out-of-plane complexes or sandwich complexes.[7] Additionally, it is known that the size and geometry of the porphyrin influence the most stable oxidation states of metal cations contained in porphyrin-type complexes. For

* Corresponding author. E-mail: sessler@mail.utexas.edu.
‡ University of Texas at Austin.
† University of Notre Dame.
⊥ Pharmacyclics, Inc.
§ University of Windsor.

(1) (a) Sessler, J. L.; Hemmi, G.; Mody, T. D.; Murai, T.; Burrell, A.; Young, S. W. *Acc. Chem. Res.* **1994**, *27*, 43−50. (b) Sessler, J. L.; Mody, T. D.; Hemmi, G. W.; Lynch, V. *Inorg. Chem.* **1993**, *32*, 3175−3187. (c) Mody, T. D.; Fu, L.; Sessler, J. L. Prog. *Inorg. Chem.* **2001**, *49*, 551−598.
(2) (a) Sessler, J. L.; Murai, T.; Lynch, V.; Cyr, M. *J. Am. Chem. Soc.* **1988**, *110*, 5586−5588. (b) Sessler, J. L.; Tvermoes, N. A.; Guldi, D. M.; Mody, T. D.; Allen, W. E. *J. Phys. Chem. A* **1999**, *103*, 787−794.
(3) (a) Rosenthal, D. I.; Nurenberg, P.; Becerra, C. R.; Frenkel, E. P.; Carbone, D. P.; Lum, B. L.; Miller, R.; Engel, J.; Young, S.; Miles, D.; Renschler, M. F. *Clin. Cancer Res.* **1945**, *5*, 739−745. (b) Viala, J.; Vanel, D.; Meingan, P.; Lartigau, E.; Carde, P.; Renschler, M. *Radiology* **1999**, *212*, 755−759. (c) Carde, P.; Timmerman, R.; Mehta, M. P.; Koprowski, C. D.; Ford, J.; Tishler, R. B.; Miles, D.; Miller, R. A.; Renschler, M. F. *J. Clin. Onc.* **2001**, *19*, 2074−2083.
(4) Guldi, D. M.; Mody, T. D.; Gerasimchuk, N. N.; Magda, D.; Sessler, J. L. *J. Am. Chem. Soc.* **2000**, *122*, 8289−8298.
(5) Shimanovich, R.; Hannah, S.; Lynch, V.; Gerasimchuk, N.; Mody, T. D.; Magda, D.; Sessler, J.; Groves, J. T. *J. Am. Chem. Soc.* **2001**, *123*, 3613−3614.
(6) Groves, J. T. *Curr. Opin. Chem. Biol.* **1999**, *3*, 226−235.

10.1021/ja012747a CCC: $22.00

Scheme 1

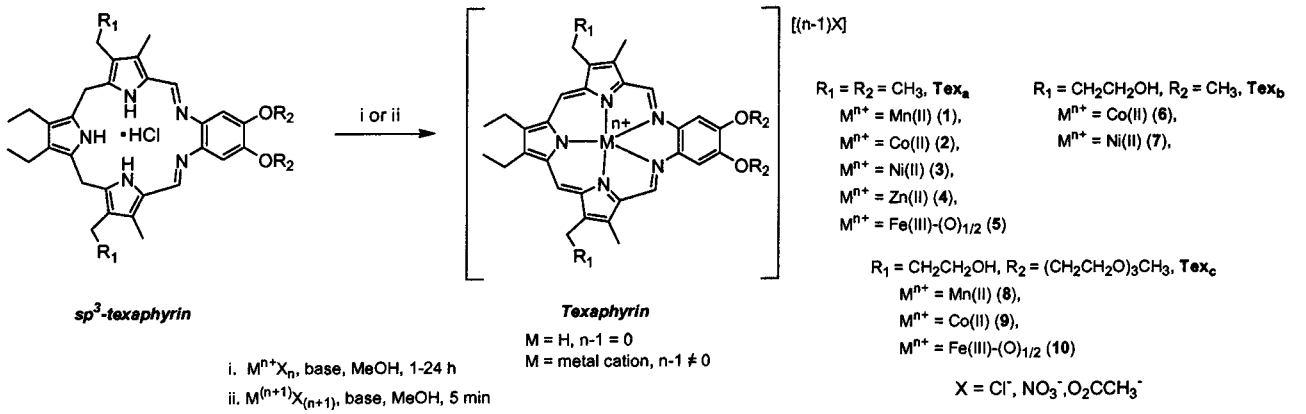

example, high-spin Mn(II) porphyrins are rapidly oxidized to the corresponding Mn(III) complexes upon exposure to oxygen, a finding that is rationalized in terms of the smaller Mn(III) cation being better able to fit within the porphyrin core. In the case of porphyrin isomers, such as porphycene,[8] and contracted porphyrins, such as corrole,[9] differences in macrocycle core size, central cavity shape, charge on the deprotonated ligand, and the electronics of the aromatic system give rise to transition metal complexes that are very different from the porphyrin complexes in terms of stability, favored oxidation state, excited-state lifetimes, etc. While a number of transition-metal complexes derived from rigid, planar penta- and hexacoordinate expanded porphyrins and "porphyrin-like" ligands have been reported,[8,10,11] one of the best studied of all expanded porphyrins, namely texaphyrin, has yet to be analyzed fully with regard to this aspect of its chemistry.

Texaphyrin complexes are generally prepared in two steps starting from the condensation of tripyrrane dialdehyde and *o*-phenylenediamine precursors. The penultimate diimine macrocycle obtained in this way is termed "sp^3-texaphyrin" (due to the hybridization state of the meso-like bridging carbon atoms).[12] During the metalation reaction with lanthanides, carried out in air, this macrocycle undergoes a four-electron oxidation.[1] The resulting aromatic texaphyrin ligand offers five nitrogens for binding, a single negative charge when deprotonated, and a cavity that is 20% larger than that of porphyrin (the center-to-nitrogen radius is ca. 2.4 Å).[1] Previously, the Mn(II) and Zn(II) complexes of a texaphyrin were prepared and their photophysical properties studied.[13] In this present study, organic-soluble complexes of Mn(II), Co(II), Ni(II), Zn(II), and Fe(III), **1**−**5**, and the water-soluble analogues **6**−**10** were prepared and characterized in the solid state through X-ray diffraction analysis and in solution through electrochemistry, EPR, and by flash photolysis.

Results

Syntheses of organic-soluble transition-metal complexes of texaphyrin, as described recently for the Mn(II) texaphyrin complex **1**,[5] have hitherto been performed by using a simultaneous oxidation/metalation method analogous to those used in the preparation of lanthanide complexes. In this method, an excess of the metal salt is stirred in an oxygenated basic methanol solution with the nonaromatic sp^3 form of the texaphyrin macrocycle corresponding to Tex$_a$ (cf., Scheme 1). As the reaction proceeds and the oxidized aromatic texaphyrin complex forms, the red solution turns yellowish green, allowing use of UV−visible spectroscopy to monitor the reactions. With use of this approach, texaphyrin complexes of Mn(II), Co(II), Ni(II), Zn(II), and Fe(III) with Tex$_a$ were synthesized (species **1**−**5** in Scheme 1), as were the more hydrophilic Co(II) and Ni(II) complexes of Tex$_b$ (structures **6** and **7**, respectively). The water-soluble Mn(II),[5] Co(II), and Fe(III) complexes **8**−**10** were also prepared, through the use of the sp^3-texaphyrin Tex$_c$ precursor, which bears solubilizing alcohol and poly(ethylene glycol) appendages.[2,14] Efforts were also made to insert copper(II) by using this same procedure. However, regardless of the copper(II) salt or reaction conditions employed, no well-characterized texaphyrin complex could be obtained.

With the first- row transition-metal salts noted above, the metal insertion and ligand oxidation reaction (Scheme 1) is complete within 1−24 h, with the specific rate depending on the identity of the metal salt. In general, metal nitrate or acetate salts react more quickly than the corresponding halides, although either can be used with no change in yield. However, it is important to note that chloride ions, stemming from either the HCl salt of the sp^3-texaphyrin or the column chromatography conditions (silica gel or reversed phase) used in the workup may partially exchange for the original anion of the metal salt. Homogeneous material may be prepared by washing organic solutions of the complex with an aqueous solution of the anion of choice or through the use of anion-exchange columns.

(7) Reviews: (a) Sanders, J. K. M.; Bampos, N.; Clyde-Watson, Z.; Darling, S. L.; Hawley, J. C.; Kim, H.-J.; Mak, C. C.; Webb, S. J. In *The Porphyrin Handbook*; Kadish, K. M., Smith, K. M., Guilard, R., Eds.; Academic Press: San Diego, CA, 2000; Vol. 3, pp 1−48. (b) *Porphyrins and Metalloporphyrins*; Smith, K. M., Ed.; Elsevier Scientific Publishing Co.: New York, 1975.
(8) (a) Sessler, J. L.; Gebauer, A.; Vogel, E. In *The Porphyrin Handbook*; Kadish, K. M., Smith, K. M., Guilard, R., Eds.; Academic Press: San Diego, CA, 2000; Vol. 2, pp 1−54. (b) Sessler, J. L.; Weghorn, S. J. *Expanded, Contracted, and Isomeric Porphyrins*; Elsevier: Oxford, 1997.
(9) (a) Erben, C.; Will, S.; Kadish, K. In *The Porphyrin Handbook*; Kadish, K. M., Smith, K. M., Guilard, R., Eds.; Academic Press: San Diego, CA, 2000; Vol. 2, pp 233−300. (b) Licoccia, S.; Paolesse, R. In *Metal Complexes with Tetrapyrrole Ligands III*; Buchler, J. W., Ed.; Springer-Verlag: Berlin, 1995; pp 71−133.
(10) (a) Sessler, J. L.; Gebauer, A.; Weghorn, S. J. In *The Porphyrin Handbook*; Kadish, K. M., Smith, K. M., Guilard, R., Eds.; Academic Press: San Diego, CA, 2000; Vol. 2, pp 55−124.
(11) (a) Sessler, J. L.; Seidel, D.; Vivian, A. E.; Lynch, V.; Scott, B. L.; Keogh, D. W. *Angew. Chem., Int. Ed. Engl.* **2001**, *40*, 591−594. (b) Sessler, J. L.; Cyr, M.; Murai, T. *Comments Inorg. Chem.* **1988**, *7*, 333−350.
(12) Sessler, J. L.; Johnson, M. R.; Lynch, V. *J. Org. Chem.* **1987**, *52*, 4394−4397.
(13) Harriman, A.; Maiya, B. G.; Murai, T.; Hemmi, G.; Sessler, J. L.; Mallouk, T. E. *J. Chem. Soc., Chem. Commun.* **1989**, 314−316.
(14) Young, S. W.; Woodburn, K. W.; Wright, M.; Mody, T.; Fan, Q.; Sessler, J. L.; Dow, W. C.; Miller, R. A. *Photochem. Photobiol.* **1996**, *63*, 892−897.

Scheme 2

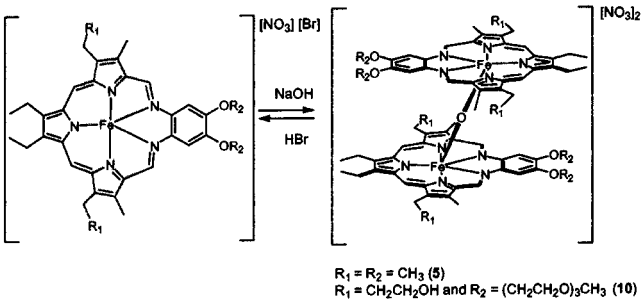

The different rates of metalation found with the various metal cations led us to consider that reduction of the transition-metal cation might contribute to the rate-limiting oxidation of the sp^3-texaphyrin macrocycle. For example, reactions employing Ni(II) and Zn(II) salts needed between 5 and 24 h to reach completion and required the presence of oxygen. On the other hand, higher valent transition-metal salts appeared to form the complex more readily and did not require oxygen. In the specific case of Mn(III) (E_{red} = 1.5 V, NHE),[5] the validity of this hypothesis was tested by carrying out the cation insertion reaction with Mn(III) acetate hydrate under argon. Starting, as usual, with the sp^3-form of the texaphyrin, the reaction was run with 5 equiv of the metal cation and standard Schlenk techniques to avoid the introduction of oxygen to the system. Under these conditions, the Mn(III) reaction again proceeded rapidly to produce the same Mn(II) texaphyrin complex **1** obtained with Mn(II) acetate under oxic conditions. However, when the corresponding Mn(II) salt was employed, the reaction proceeded much more slowly when run under argon than in the presence of air.

The synthesis of an iron texaphyrin complex provided another example wherein the metal cation acted as an oxidizing agent. An initial product, displaying a λ_{max} of 717 nm in the so-called Q-band spectral region, was observed upon reaction of the reduced sp^3 form of texaphyrin with Fe(III) nitrate under oxygen-free conditions or with Fe(II) acetate, heated to reflux while open to air. This initial species is believed to be an Fe(II) complex, analogous to the Mn(II) complex obtained with Mn(III) salts. Thus far, however, efforts to isolate and purify this putative Fe(II)-Tex_a complex have proved unsuccessful, due to its facile conversion to the corresponding μ-oxo dimer, **5**. The identity of this latter species was confirmed via X-ray diffraction analysis (cf., next section.)

μ-Oxo dimers, analogous to **5**, are common products in iron porphyrin chemistry, with Fe(II) porphyrins being readily oxidized to the corresponding Fe(III)-oxo dimers upon exposure to air.[15] In porphyrin chemistry, it is known that the μ-oxo bond can be cleaved by treatment with hydrochloric or hydrobromic acid to yield the corresponding monomeric Fe(III) complex. It appears that this method can be used to cleave the μ-oxo bond in **5**, as judged by observing the changes in its UV−vis spectrum as aqueous HBr was added (Scheme 2 and Figure 1). Thus far, however, it has not proved possible to convert the dimer into the corresponding monomer completely, as the texaphyrin macrocycle is susceptible to acid-induced decomposition in solutions below pH 4.

As was observed for the lanthanide(III) complexes of texaphyrin,[1] all the transition-metal complexes reported here proved

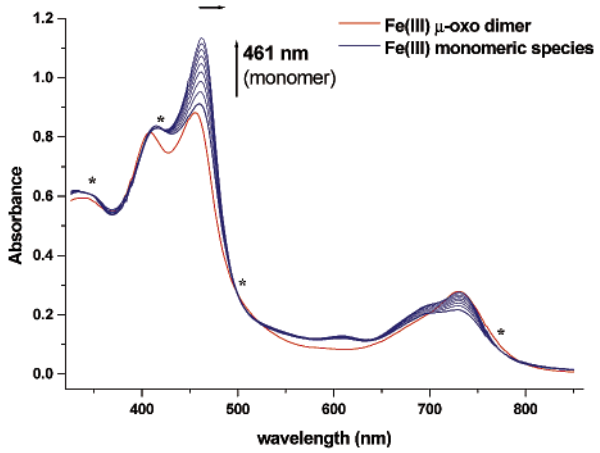

Figure 1. UV−vis spectral changes associated with the aqueous HBr-induced conversion of $([Fe(Tex_b)]_2O)(NO_3)_2$ to its monomeric form in methanol (7.5×10^{-5} M) at room temperature over the course of 45 min, with spectra taken at 5 min intervals. Isosbestic points are observed at 344, 420, 500, and 776 nm. Total conversion to the corresponding monomeric complex, Fe(Tex_b)Br, was not observed.

fairly stable in the solid state at room temperature and completely stable when stored at −20 °C. Decomposition is observed in solution if the complexes are exposed to light or heat for extended periods of time. As a consequence, most manipulations were carried out in the absence of light and at room temperature. Additionally, solutions of these complexes, particularly the Ni(II) and Zn(II) complexes, were found to be unstable at low pH (<4). This latter instability is thought to reflect protonation of the imine nitrogen followed by hydrolysis and decomposition. The stability of solutions of the Mn(II) and Co(II) complexes, at a concentration of approximately 1.5×10^{-4} M, was monitored over a period of 10 days while kept at ambient temperature and covered from light to prevent photobleaching. Complexes that had been dissolved in organic solvents such as DMSO and methanol showed no significant change in absorbance over this period of time. However, the Co(II) complex **9**, as well as the Co(II) complex of Tex_b, **6**, formed slightly acidic solutions (pH <6) in water. In this acidic medium, these complexes were unstable and their characteristic UV−vis signatures disappeared completely within 24 h. On the other hand, in buffered aqueous solutions at pH >7.2, complex **9** appeared to be stable for at least a day. Solutions of Mn-Tex, whether formulated in water or neutral buffer, appeared to be stable over this time period as well.

Solutions of **10** in different solvents are stable over several hours. However, prolonged storage results in entropically driven monomerization, as judged by the appearance of spectral features similar to those shown in Figure 1, even in the absence of added acid. With use of a procedure in which dilute methanol solutions of **10** were monitored spectroscopically for over 100 h, the rate constant for the monomerization reaction in methanol (k_{mono}) was found to be $(7.5 \pm 2.3) \times 10^{-6}$ s^{-1}.[16] It was also noted that μ-oxo-dimeric-Fe(III) texaphyrins gradually degrade in polar aprotic solvents, such as DMSO and DMF, that have strong ligating properties.

Single-Crystal X-ray Diffraction Analysis. All of the Tex_a complexes, with the exception of the Ni(II) texaphyrin complex,

(15) (a) Chin, D.-H.; Del Gaudio, J.; La Mar, G. N.; Balch, A. L. *J. Am. Chem. Soc.* **1977**, *99*, 5486−5388. (b) Kurtz, D. M., Jr. *Chem. Rev.* **1990**, *90*, 585−606.

(16) Gerasimchuk, N. N.; Mokhir, A. A.; Rodgers, K. R. *Inorg. Chem.* **1998**, *37*, 641−5650.

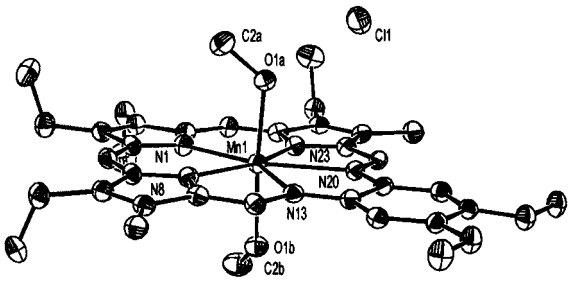

Figure 2. Complex **1**$(MeOH)_2Cl$ crystallized from MeOH. An additional MeOH molecule contained in the lattice is not shown.

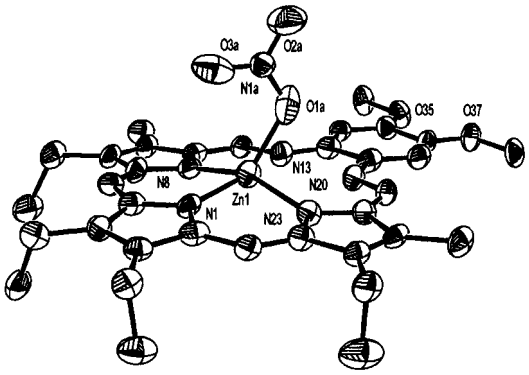

Figure 3. Structure of complex **4**. A disordered chloride anion, complexed to the Zn(II) center and in the same position as the nitrate group, is not shown.

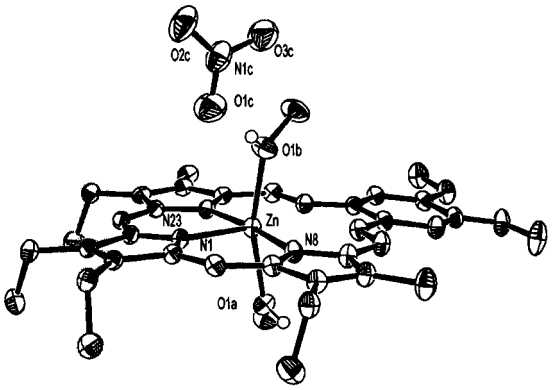

Figure 4. Structure of complex **4**$(MeOH)_2NO_3$.

3, were characterized by single-crystal X-ray diffraction analysis. The resulting structures are shown as Figures 2−5, with important bond lengths and angles listed in Table 1. Inspection of these figures reveals that the structures in question can be grouped into two classes, those in which the cation is ligated by all five texaphyrin nitrogens (complexes **1**, **2**, and **5**) and those wherein only three nitrogen centers are coordinated (complex **4**). Further, the structures can be categorized on the basis of whether the apical coordination sites are occupied by counteranions (complexes **1**, **4**, and **5**) or solvent, with the counteranion hydrogen bonded to the solvent or free in the lattice (**1**$(MeOH)_2Cl$, **2**$(MeOH)_2Cl$, and **4**$(MeOH)_2Cl$.) The fact that this second type of structure is observed in the solid state leads us to propose that the anions are most probably not coordinated in polar solutions. In those structures in which the anion is coordinated, the metal is generally located slightly out of the plane of the texaphyrin, toward the anion, with no additional axial ligand. Alternatively, in those structures wherein solvent

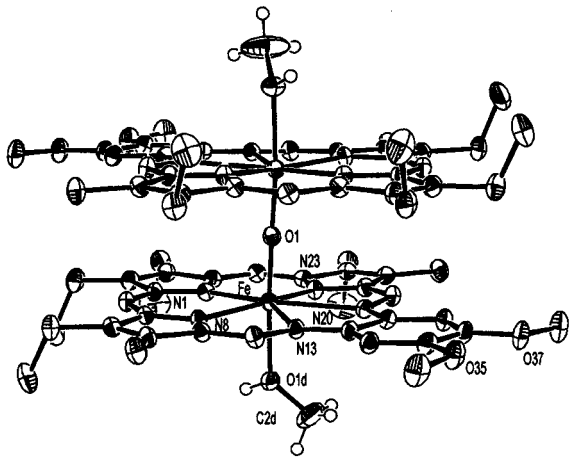

Figure 5. Structure of the μ-oxo Fe(III) texaphyrin dimer, **5**. Two noncoordinating nitrate anions contained in the lattice are not shown.

molecules serve as axial ligands, the metal generally resides within the mean N_5 plane. In these instances, two solvent molecules are bound to the metal center and are seen to occupy positions above and below the texaphyrin core. The M−N bond lengths for the anion-bound species are all slightly longer, due to the out-of-plane displacement of the unsymmetrically coordinated metal. Thus, for most of the metal complexes reported here, two different coordination numbers have been observed in the solid state. These two types of geometry were also observed for Cd(II) complexes of texaphyrin, [Cd-Tex(benzimidazole)NO_3] and [Cd-Tex(pyridine)$_2NO_3$].[17] Against this background of generalities, each of the individual structures will now be discussed in detail.

The structure of the chloride-bound species of the Mn(II) complex **1** has been reported previously.[5] The geometry around the 6-coordinate metal center is best described as highly distorted octahedral. The Mn(II) center is located 0.371 Å above the mean N_5 plane of the texaphyrin core and is not centered among the five bonding nitrogens. Rather, it is displaced toward the pyrrolic nitrogens, N_1, N_8, and N_{23}, with Mn−N bond lengths that are 0.156−0.313 Å shorter than the average of the Mn−N imine bond lengths, Mn−N_{13} and Mn−N_{20}. On the other hand, in the structure of the solvent-coordinated manganese(II) texaphyrin, **1**$(MeOH)_2Cl$, displayed in Figure 2, the Mn(II) atom is located within the N_5 plane. Since the Mn(II) atom is not centrosymmetric within the macrocycle, however, the geometry about the metal can be described as distorted pentagonal bipyramidal. The Mn(II) center is again displaced toward the tripyrrolyldimethene portion of the macrocycle, with two shorter Mn−N bonds to the outer pyrrolic nitrogens, N_8 and N_{23}, and a slightly longer (by 0.17 Å) Mn−N_1 bond to the central pyrrolic nitrogen. Two methanol molecules are coordinated in the axial positions with the Mn−O bond lengths (average of 2.217 Å) being shorter than all five Mn−N bonds. The bonds to the two imine nitrogens, N_{13} and N_{20} (0.24 Å longer than the shortest Mn−N_{pyr} bond), are particularly long and define a coordination diameter that is longer than the sum of the ionic radii for even 7-coordinate Mn(II).[18] As a result, the contribution to bonding from these positions is presumed to derive mainly from ion−dipole-type interactions and is likely to be minor. For compari-

(17) Sessler, J. L.; Murai, T.; Lynch, V. *Inorg. Chem.* **1989**, *28*, 1333−1341.
(18) Huheey, J. E.; Keiter, E. A.; Keiter, R. L. *Inorganic Chemistry*, 4th ed.; HarperCollins College Publishers: New York, 1993.

Table 1. Selected Bond Lengths (Å) and Angles (deg)[a]

	1(Mn)[b]	**1**(Mn(MeOH)$_2$)	**2**(Co(MeOH)$_2$)	**4**(Zn)	**4**(Zn(MeOH)$_2$)	**5**(Fe)
M−N$_1$	2.383(3)	2.409(2)	2.335(4)	2.066(6)	2.139(2)	2.321(2)
M−N$_8$	2.233(3)	2.233(3)	2.172(5)	2.132(6)	2.143(2)	2.202(2)
M−N$_{13}$	2.558(3)	2.476(2)	2.514(2)	2.929(6)	2.779(2)	2.501(2)
M−N$_{20}$	2.520(3)	2.464(2)	2.533(2)	2.894(6)	2.800(2)	2.494(2)
M−N$_{23}$	2.226(3)	2.239(3)	2.179(6)	2.121(6)	2.133(2)	2.199(2)
Δ(N5)[c]	0.371	0	0	0.38	0	0.112
M−X(axial)	2.4115(11) (chloride)	2.217(2) (av MeOH)	2.116(4) (av MeOH)	1.958(15) (nitrate)	2.137(2) (av MeOH)	1.7525(5) (oxo)
N$_1$−M−N$_8$	79.34(11)	79.19(10)	80.8(2)	88.3(2)	86.47(8)	80.36(7)
N$_8$−M−N$_{13}$	67.64(10)	69.12(9)	68.50(2)			68.54(7)
N$_{13}$−M−N$_{20}$	61.38(9)	63.95(7)	61.32(2)			61.79(7)
N$_{20}$−M−N$_{23}$	68.01(10)	69.18(9)	68.89(2)			69.02(7)
N$_{23}$−M−N$_1$	78.60(11)	78.56(10)	80.5(2)	87.5(2)	87.53(8)	79.83(7)
N$_8$−M−N$_{23}$	151.26(11)	157.73(8)	161.28(2)	157.3(2)	173.65(8)	159.31(7)
X−M−X		173.56(9)	172.87(13)		162.54(8)	174.05(6)
N$_1$−M−X	102.64(8)	92.98(9)	93.7(2)	126.6(5)	100.07(8)	96.14(5) (O$_1$)
		93.39(9)	93.3(2)		96.59(8)	89.64(7)

[a] The pyrrolic nitrogens are labeled as N$_1$, N$_8$, and N$_{23}$. The imine nitrogens are labeled as N$_{13}$ and N$_{20}$. [b] Reference 5. [c] The distance to the metal cation from the mean plane through the five-coordinating nitrogen atoms of the macrocycle.

son, the average Mn(II)−N bond length in the analogous porphyrin complex, square-pyramidal [Mn(TPP)(1-methylimidazole)], is 2.128 Å.[19] Notably, the Mn(II) cation, in this structure and others, is too large to sit within the plane of the porphyrin, and as such, it does not coordinate a second axial ligand, even in the presence of good donor solvents such as pyridine, because the porphyrin ring blocks such interactions. Texaphyrin, with metal−nitrogen distances that are considerably longer than those found in most Mn(II) complexes, not just porphyrins,[20] has ample room for the Mn(II) cation, along with one or more axial ligands. In the case of the previously published chloride structure, the axial ligand is Cl^-. In the solvated structure shown in Figure 2, the chloride counteranion is not coordinated to the metal center. Rather, it is hydrogen bonded to one of the methanol molecules and to a second molecule of **1**, in a hydrogen-bonded chain network that continues through the crystal.

Only one structure of the cobalt texaphyrin, **2**, has been successfully solved by X-ray diffraction analysis; it was found to be essentially isostructural to the solvated Mn structure described above with a noncoordinated chloride counterion. The smaller Co(II) cation is located even closer to the three pyrrolic nitrogens than the Mn(II) cation. The difference between the shortest Co−N pyrrole bonds (N$_8$ and N$_{23}$) and the longer Co−N$_{imine}$ bonds is now up to approximately 0.35 Å. Again, the Co−N$_{imine}$ bond lengths (average 2.52 Å) are much larger than the sum of the ionic radii. The Co−N$_{imine}$ bonds, to the extent they exist, must contribute only marginally to complex stabilization.

The solid-state structure of the Zn texaphyrin, **4**, shown in Figure 3, as well as its MeOH-solvated structure **4**(MeOH)$_2$NO$_3$, shown in Figure 4, provide the first examples of texaphyrin acting as a tridentate ligand. In these instances, the trend toward lengthened, and presumably weakened M−N$_{imine}$ bonds manifest in the Mn(II) and Co(II) structures has become enhanced to the point where it is no longer reasonable to consider the metal−imine nitrogen interaction, if any, as coordinate covalent bonding. On the other hand, in both **4** and **4**(MeOH)$_2$NO$_3$, Zn−N bond lengths consistent with strong bonding to the formally monoanionic tripyrrolyldimethene fragment are observed. In the specific case of **4**, the shortest Zn−N bond lengths are to the two neighboring pyrrole nitrogens, N$_1$ and N$_{23}$, with the third M−N$_8$ bond being slightly longer. In this complex, the distorted tetrahedral coordination sphere is completed by the anion, which in this crystal was mixed as either chloride or nitrate (only the nitrate anion is shown in Figure 3 for clarity.) The metal center sits 0.38 Å above the mean plane toward the anion. Notably, no ruffling is observed, as is found in porphyrin complexes coordinated to smaller metal cations such as Ni(II). The Zn−N$_1$ bond length and axial displacement of this Zn(II) texaphyrin complex are surprisingly similar to those of [Zn(TPP)(OH$_2$)], which has a Zn−N(pyrrole) bond length of 2.066 Å and an out-of-plane displacement of 0.36 Å.[21] However, the other two Zn−N(pyrrole) bond lengths in **4** are longer than any observed in Zn(II) porphyrin structures.

Consistent with the above, in the solvent-coordinated structure (Figure 4), the distances from the Zn(II) center to the tripyrrolyldimethene nitrogens N1, N8, and N23 are shorter than those found in the aforementioned Mn(II) and Co(II) complexes. However, in this structure, the Zn atom is located within what is an essentially planar texaphyrin ring. As a result of the two coordinated solvent molecules, the metal center exists in a trigonal bipyramidal ligand environment. Nonetheless, the N$_8$−Zn−N$_{23}$ bond angle of 173.65(8)°, nearly linear, would be inconsistent with an ideal trigonal bipyramidal geometry. This suggests that a remnant of imine bonding may still exist in this solvated form. Such a coordination environment is, not surprisingly, without precedent in the case of Zn(II) porphyrin complexes. Further, the close association with solvent molecules is also without precedent. Zinc porphyins, as bis(solvated) species are generally not observed in solution, but may occur in the solid state only as the result of crystal-packing forces. As a result, long bonds are usually seen. For instance, the Zn−O bonds in [Zn(TPP)(THF)$_2$] average 2.380 Å.[22] This is far longer then the average Zn−MeOH bond length of 2.137 Å seen in **4**(MeOH)$_2$NO$_3$.

(19) Kirner, J. F.; Reed, C. A.; Scheidt, W. R. *J. Am. Chem. Soc.* **1977**, *99*, 2557−2563.
(20) A search of the Cambridge Structural Database revealed no complexes of Mn(II), with macrocyclic or acyclic ligands, with Mn−N bonds longer than those reported herein.
(21) Cheng, B.; Scheidt, W. R. *Inorg. Chim. Acta* **1995**, *237*, 5−11.
(22) Schauer, C. K.; Anderson, O. P.; Eaton, S. S.; Eaton, G. R. *Inorg. Chem.* **1985**, *24*, 4082−4086.

The symmetry-generated structure of the iron(III) μ-oxo texaphyrin dimer, **5**, is displayed in Figure 5. The two noncoordinated nitrate counteranions are not shown. The geometry about each Fe(III) center is similar to that in the bis(solvated) manganese(II) structure, **1**$(MeOH)_2Cl$, and the nearly isostructural cobalt(II) complex. As in the latter complexes, the iron cation in **5** is located closer to the pyrrolic nitrogens than to the imine nitrogens, but maintains a similar distance of 2.3−2.4 Å from the nitrogen of the central pyrrole. Further, the metal center lies nearly within the penta-aza plane of the texaphyrin ring, being displaced only slightly (by 0.112 Å) toward the bridging-oxo ligand. The Fe−O bond distance, at 1.75 Å, is similar to that observed in Fe(III) μ-oxo porphyrins.[23] On the other hand, the Fe−N distances in **5**, ranging from 2.199 to 2.501 Å are, on average, much longer than those in analogous porphyrin complexes (i.e., Fe−N in $[Fe(TPP)]_2O$ is 2.087 Å).[23] The face-to-face texaphyrin macrocycles are situated so that the benzene-ring portion of one is under the tripyrrolyldimethene portion of the other. Since the Fe atoms are not centered within the texaphyrin, this leads to a slight angle between the linear Fe−O−Fe bond and the equatorial plane of each texaphyrin. Each Fe(III) atom is also coordinated axially by a MeOH molecule. The structure that results is thus an interesting compromise between the 6-coordinate anion-bound and the 7-coordinate bis-solvated structures observed in the case of Mn(II) and Co(II) texaphyrin complexes (vide supra), despite the formally trivalent charge on the cations in the dimer.

Solution Magnetic Moment Determinations. To understand more fully the electronic structure of the transition metal texaphyrins **1**−**5**, the room temperature, spin-only magnetic moment of each paramagnetic complex was determined in methanol solution by using the Evans method.[24] The values deduced in this way matched well with those calculated for appropriate high-spin reference complexes.[25] For instance, the manganese(II) complex **1** produced a $\mu_{eff} = 5.91\ \mu_B$, as would be expected for a spin $^5/_2$ state. By way of comparison, both 4-coordinate and 5-coordinate Mn(II) porphyrins exist in a high-spin ($S = {}^5/_2$) state, while six-coordinate Mn(II) porphyrin complexes are generally low spin.[26] Similarly, the Co(II) texaphyrin, **2**, displayed a $\mu_{eff} = 4.18\ \mu_B$, a value consistent with a high-spin ($S = {}^3/_2$) d^7 system. Cobalt(II) porphyrins, on the other hand, generally exist as low-spin ($S = {}^1/_2$) complexes.[7] The nickel(II) texaphyrin complex, **3**, gave a spin-only magnetic moment of $\mu_{eff} = 2.86\ \mu_B$, exactly the value expected for a high-spin ($S = 1$) d^8 system. This finding leads us to conclude that the Ni(II) cation in **3** is not in a square-planar coordination environment typical of Ni(II) porphyrins, particularly in the solvent used for the study, methanol. The presence of a paramagnetic Ni(II) center is rationalized in terms of either a five- or six-coordinate geometry. While the existence of five-coordinate high-spin Ni(II) porphyrins has not been clearly established,[27] paramagnetic octahedral Ni(II) porphyrin complexes are well-known.[28] Five-coordinate paramagnetic Ni(II) complexes of multidentate nitrogen ligands, generally with square-pyramidal geometry, have been reported for several systems, including monothiaporphyrin.[29] The expanded core of texaphyrin could accommodate either geometry. The Fe(III) dimer, **5**, displayed a $\mu_{eff} = 6.01\ \mu_B$ per molecule of complex. This is considerably lower than expected for two independent Fe^{3+} high-spin metal centers, and is interpreted in terms of a strong antiferromagnetic interaction between iron(III) atoms established via the bridging oxygen atom.

To support further the electronic assignments made through the analysis of magnetic moments, EPR analyses of Mn-Tex_a (**1**), Co-Tex_a (**2**), and Ni-Tex_a (**3**) complexes were carried out at 4 K in protic and nonprotic frozen glasses obtained from solutions of these complexes in ethanol, toluene, and DMF. The spectra of the Mn(II) and Co(II) complexes exhibited signals that were typical for the high-spin forms of these cations. For instance, the EPR spectra of complex **1** were characterized by signals at three different *g*-values, namely 1.822, 4.094, and 11.03 for g_x, g_y, and g_z, respectively. Each signal exhibited hyperfine structure in 6-line patterns characteristic of Mn(II) in a rhombic environment.[30] Accordingly, complex **1** appears to be a compound with strong *g*-factor anisotropy. The g_x and g_y signals also displayed additional but not well-resolved splittings that are tentatively assigned as hyperfine splittings involving the nitrogen atoms of the macrocyclic core. The EPR spectrum of the Co(II) complex **2** revealed one poorly resolved signal at a *g*-value of approximately 4.1. However, the Ni(II) complex **3** gave rise to a good quality spectrum, with signals at *g*-values of 2.239 and 3.702 being readily observed. This supports the notion that the Ni(II) complex has a coordination geometry such that the metal center is in a d^8 non-Kramer's doublet electronic configuration.

UV−Vis Spectroscopic Studies. All reactions were monitored with UV−vis spectroscopy. Intensely colored green-yellow solutions of the monomeric transition-metal complexes gave spectra that are analogous, in terms of shape and intensity, to those of the lanthanide(III) texaphyrins.[1] However, the exact positions of the bands for the transition-metal species are for the most part blue-shifted as compared to those of the lanthanide complexes. The spectra of methanol solutions of the Tex_a complexes **1**−**4** shown in Figure 6, identical in shape to the spectra of their Tex_b and Tex_c congeners, consist of two main bands with small shoulders, a Soret-like band at shorter wavelengths and a Q-like band at longer wavelengths. These absorbances are analogous to the optical transitions observed and theoretically well-established for metalloporphyrins.[31]

(23) (a) Scheidt, W. R. In *The Porphyrin Handbook*; Kadish, K. M., Smith, K. M., Guilard, R., Eds.; Academic Press: San Diego, CA, 2000; Vol. 3, pp 49−112. (b) Hoffman, A. B.; Collins, D. M.; Day, V. W.; Fleischer, E. B.; Srivastava, T. S.; Hoard, J. L. *J. Am. Chem. Soc.* **1972**, *94*, 3620−3626.

(24) (a) Crawford, T. H.; Swanson, J. *J. Chem. Educ.* **1971**, *48*, 383−386. (b) Evans, D. F. *J. Chem. Soc.* **1959**, 2003−2005.

(25) Drago, R. S. *Physical Methods for Chemists*, 2nd ed.; W. B. Saunders Co.: Philadelphia, PA, 1993.

(26) (a) Reed, C. A.; Kouba, J. K.; Grimes, C. J.; Cheung, S. K. *Inorg. Chem.* **1978**, *17*, 2666−2670. (b) Gonzalez, B.; Kouba, J.; Yee, S.; Reed, C. A.; Kirner, J. F.; Scheidt, W. R. *J. Am. Chem. Soc.* **1975**, *97*, 3247−3249. (c) Kirner, J. F.; Reed, C. A.; Scheidt, W. R. *J. Am. Chem. Soc.* **1977**, *99*, 2557−2563. (d) Harmer, H. R.; Reimer, K. J.; Smith, D. W.; James, B. R. *Inorg. Chim. Acta* **1989**, *166*, 167−169.

(27) (a) Walker, F. A.; Hui, E.; Walker, J. M. *J. Am. Chem. Soc.* **1975**, *97*, 2390−2397. (b) Caughey, W. S.; Fujimoto, W. Y.; Johnson, B. P. *Biochemistry* **1966**, *5*, 3830−3843.

(28) (a) Senge, M. *J. Porphyrins Phthalocyanines* **1998**, *2*, 107−121. (b) Vidal-Ferran, A.; Bampos, N.; Sanders, J. K. M. *Inorg. Chem.* **1997**, *36*, 6117−6126. (c) Hobbs, J. D.; Majunder, S. A.; Luo, L.; Sickelsmith, G. A.; Quirke, J. M. E.; Medforth, C. J.; Smith, K. M.; Shelnutt, J. A. *J. Am. Chem. Soc.* **1994**, *116*, 3261−3270. (d) Kirner, J. F.; Garofala, J.; Scheidt, W. R. *Inorg. Nucl. Chem. Lett.* **1975**, *11*, 107−112.

(29) (a) Latos-Grażyński, L.; Lisowski, J.; Olmstead, M.; Balch, A. L. *Inorg. Chem.* **1989**, *28*, 1183−1188. (b) Curtis, N. F. *Aust. J. Chem.* **1988**, *41*, 957−961. (c) Masood, M. A.; Hodgson, D. J. *Inorg. Chem.* **1994**, *33*, 3038−3042.

(30) (a) Pilbrow, J. R. *Transition Ion Electron Paramagnetic Resonance*; Clarendon Press: Oxford, 1990; p 717. (b) Chandra, S. K.; Chakravorty, A. *Inorg. Chem.* **1992**, *3*, 760−765. (c) Reed, G. H.; Cohn, M. *J. Biol. Chem.* **1970**, *245*, 662.

Table 2. UV−Vis Data for Metallotexaphyrin Solutions

texaphyrin complex	ionic radii (pm)[a]	solvent	λ_{max} (nm, (log e)) Soret-like, Q-like
Mn^{2+}-Tex_a (**1**)	104 (HS, 7-coord)	MeOH	460 (4.96), 727 (4.51)
Mn^{2+}-Tex_a (**1**)	104	CH_2Cl_2	464 (4.43), 734 (4.09)
Mn^{2+}-Tex_c (**6**)	104	MeOH	463 (4.91), 732 (4.45)
Mn^{2+}-Tex_c (**6**)	104	DMSO	468 (4.90), 731 (4.42)
Mn^{2+}-Tex_c (**6**)	104	H_2O	461 (4.77), 730 (4.28)
Mn^{2+}-Tex_c (**6**)	104	$CHCl_3$	467 (4.78), 740 (4.29)
Fe^{2+}-Tex_a (monomer)	78.5 (HS, 6-coord)	MeOH	459[b], 717[b]
Fe^{3+}-Tex_c μ-oxo dimer (**10**)	78.5 (HS)	MeOH	408 (4.90), 450 (4.88), 732 (4.34)
Co(II)-Tex_a (**2**)	88.5 (HS, 6-coord)	MeOH	457 (4.75), 713 (4.56)
Ni(II)-Tex_a (**3**)	83	MeOH	457 (4.98), 704 (4.56)
Zn(II)-Tex_a (**4**)	88 (6-coord)	MeOH	456 (4.77), 704 (4.30)
Cd(II)-Tex_c[c]	110 (8-coord)	MeOH	465 (4.98), 734 (4.55)
Lu(III)-Tex_c[c]	103 (9-coord)	DMSO	478 (5.03), 731 (4.58)

[a] Reference 18. [b] Extinction coefficient could not be determined since the complex was not isolated. [c] Reference 4.

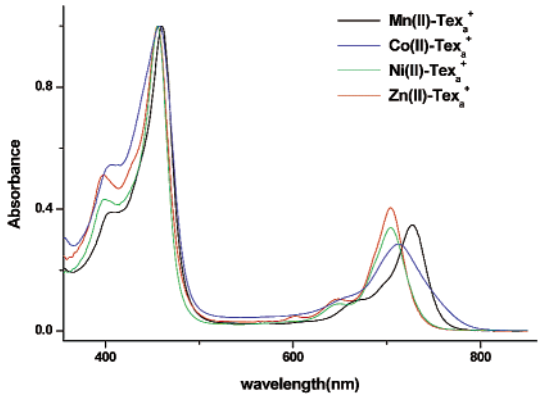

Figure 6. UV−vis spectra of monomeric texaphyrin complexes **1**−**4** recorded in methanol. The absorbance scale of each spectrum was normalized to 1 to permit the overlay plot. Extinction coefficients are reported in Table 2.

In the UV−vis spectra of the texaphyrin complexes **1**−**10**, the positions of both the Soret-like and, more so, the Q-like bands are seen to shift with the identity of the metal atom and, to a lesser degree, the choice of solvent. The μ-oxo-dimer Fe(III) texaphyrin, **10**, displays hypsochromicity and broadening in its UV−vis spectrum, similar to what is observed in analogous porphyrin systems.[31] A representative sample of UV−vis data is collected in Table 2, allowing a comparison of the shifts observed upon changing the ligand from Tex_a to Tex_c, exchanging the metal cation, and varying the solvent. Notably, for any given metal and solvent, the use of the differentially substituted but electronically similar texaphyrin ligands leads to very little change in the Soret-like band (3 nm) and in the Q-like band (5 nm), and a negligible change in the extinction coefficient. This is not unexpected but does facilitate other comparisons involving changes in solvent and cation. Solvent effects, although small, are still appreciable. For instance, the position of the Soret-like band shifts from 467 to 461 nm when the complex Mn-Tex_c is recorded in $CHCl_3$ as compared to H_2O, with the difference in the Q-like band, more red-shifted in the case of the spectrum recorded in $CHCl_3$, being 10 nm. These modest shifts provide evidence of a solvatochromic effect;[32] that is, they are consistent with charge-transfer contributions to both the Q-band, or $S_0 \rightarrow S_1$ low energy transition, and the Soret band, or $S_0 \rightarrow S_2$ higher energy transitions, in the texaphyrin chromophore. Such charge-transfer effects are, in turn, characteristic of some degree of covalent bonding involving, in this instance, the deprotonated form of the macrocycle and the metal cation. By contrast, a comparison of the monomeric complexes **1**−**4** reveals that there is a fairly dramatic 23 nm blue-shift of the Q-like band as the metal ion is varied across the late first-row transition metals from Mn(II) to Zn(II).

Photophysical Spectroscopic Studies. The effect of transition metal cation binding on the photophysics of the ligand chromophore was investigated by using standard time-resolved techniques. Singlet and triplet lifetimes and fluorescent quantum yields for representative compounds are compiled in Table 3. These data are consistent with the above characterization of all of the cations, with the exception of Zn(II), occupying a high-spin state. Singlet and triplet lifetimes of the paramagnetic species were found to decrease by a factor of 5 and 1000, respectively, in comparison to the diamagnetic Zn(II) complex. Similarly, fluorescent quantum yields are 100-fold lower in the paramagnetic derivatives. These data are reminiscent of the photophysical properties of paramagnetic lanthanide texaphyrins seen previously and ascribed to enhancement of internal conversion and intersystem crossing rates.[4] The fluorescent quantum yield of the Zn(II) texaphyrin was somewhat lower than that found for the Y(III) texaphyrin, despite having a lower atomic number (and hence reduced heavy atom effect). On the other hand, the triplet quantum yield for Zn-Tex_a was found to be essentially analogous to that of Y-Tex_c (0.59 vs 0.563[4]), with the corresponding singlet oxygen quantum yields for these two species both being ca. 0.54. This could be due to a higher level of vibrational freedom in the Zn(II) derivative; it could also reflect a stronger covalent bonding between the metal and the texaphyrin macrocycle in the Zn complex than in the other metal complexes.

Electrochemistry. Each of the transition metal complexes **1**−**10** was analyzed by cyclic voltammetry. Given the presence of redox active metal cations in certain of the complexes, the possibility of detecting metal-centered waves was anticipated. However, the cyclic voltammograms of the transition-metal texaphyrin complexes are qualitatively similar to those recorded previously for the corresponding lanthanide(III) complexes, for which two ligand-centered reductions are observed when scanned over the −200 to −800 mV range.[2,33] Two reduction potentials, at most, were also measured for the transition-metal

(31) (a) Gouterman, M. In *The Porphyrins*; Dolphin, D., Ed.; Academic Press: New York, 1978; Vol. III, pp 1−165. (b) Buchler, J. W. In *The Porphyrins*; Dolphin, D., Ed.; Academic Press: New York; Vol. I, pp 390−483.
(32) (a) Kosower, E. M. *J. Am. Chem. Soc.* **1961**, *83*, 3142−3148. (b) Kosower, E. M. In *The Enzymes*; Boyer, P. D., Lardy, H., Myrbach, A., K., Eds.; Academic Press: New York, 1960; Vol. 3. (c) Gerasimchuk, N. N. Ph.D. Thesis, The University of Kansas, 1997.

Table 3. Photophysical Data for Metallotexaphyrin Complexes

	lifetime (ps)		triplet lifetime		fluorescence	singlet
	singlet	fluorescence	deaerated	aerated	quantum yields	energy (eV)
Mn (**1**)	56	[a]	1.03 ns		5×10^{-5}	1.66
Co (**2**)	61	[a]	1.1 ns		6×10^{-5}	1.66
Ni (**3**)	75	[a]	2.5 ns		1.4×10^{-4}	1.69
Zn (**4**)	302	330	5.5 μs	410 ns	6.9×10^{-3}	1.67
Fe (**5**)	~50	[a]	[a]		$<5 \times 10^{-5}$	1.60
Y-Tex$_c$[b]	1652	1298	187 μs	4.0 μs	0.04	1.60
Cd-Tex$_c$[b]	675	715	122 μs	4.6 μs	0.015	1.6

[a] Not detected. [b] Reference 4.

Table 4. Electrochemical Reduction Potentials for Texaphyrin Complexes **1**−**10** in DMSO Solution (Ag/AgCl reference, 0.1 M TBAP)

complex	metal ion	concn, M	$^1E_{1/2}$, mV	$^2E_{1/2}$, mV
1(CH_3COO)	Mn(II)−	2.10×10^{-3}	−571 ± 2.6	−1008 ± 3
2(NO_3)	Co(II)	2.8×10^{-3}	−577 ± 2.1	−843 ± 9
3(NO_3/Cl)	Ni(II)	1.8×10^{-3}	−490 ± 3.5	−1190 ± 8 (nr)[a]
4(NO_3/Cl)	Zn(II)	1.8×10^{-3}	−454 ± 1	−1513 ± 3.8 (nr)[a]
5$(Cl)_2$	Fe(III)(dimer)	6.2×10^{-4}	−561 ± 2	*b*
6(CH_3COO)	Co(II)	1.8×10^{-3}	−565 ± 3.3	−846 ± 3.2
7(NO_3)	Ni(II)	1.9×10^{-3}	−498 ± 3.6	*b*
8(CH_3COO)	Mn(II)	9.8×10^{-4}	−560 ± 1.4	−1001 ± 0.5 (nr)[a]
9(NO_3)	Co(II)	1.5×10^{-3}	−480 ± 3.5	−1380 ± 4.5
9(CH_3COO)	Co(II)	1.3×10^{-3}	−574 ± 2.7	−867 ± 6
10$(CH_3COO)_2$	Fe(III)	8.5×10^{-4}	−607 ± 3.5	−996 ± 2.5
Cd(Tex$_c$)(CH_3COO)[c]	Cd(II)	9.6×10^{-4}	−461 ± 3.8	−936 ± 7.6
Lu(Tex$_c$)$(CH_3COO)_2$[c]	Lu(III)	2.4×10^{-3}	−237 ± 3.9	−731 ± 9
Gd(Tex$_c$)$(CH_3COO)_2$[c]	Gd(III)	2.5×10^{-3}	−294 ± 0.3	−732 ± 9
MnTPP[c] (in DMF)[d]	Mn(II)		−1290	*b*
CoTPP[c] (in DMF)[d]	Co(II)		−778	−1880
NiTPP[c] (in DMF)[d]	Ni(II)		−1170	−1710
ZnTPP[c] (in DMF)[d]	Zn(II)		−1280	−1700

[a] (nr): estimate; reduction is nonreversible. [b] Value could not be determined due to the absence of a cathodic return wave (i.e. irreversible behavior). [c] Reference 4. [d] References 35−38.

texaphyrins and are listed in Table 4. The first reduction waves of complexes **2**, **3**, **5**, **6**, and **8**, are best described as quasi-reversible to nonreversible. The second reduction is nonreversible in the case of **3**, **4**, **5**, **7**, and **8**. Reversible behavior for both reduction processes was exhibited by complexes **2**, **8**, and **10**, as shown in Figure 7. Efforts to improve reversibility by performing the measurements in pyridine[34] were unsuccessful. No waves corresponding to oxidation of the texaphyrin complexes, either at the ring or at the coordinated metal center, were found within the scan limits of the solvent.

As can be seen from an inspection of Table 4, all of the transition metal complexes considered in the present study proved much easier to reduce than their tetraphenylporphyrin analogues,[35−38] the potentials for which are also listed in Table 4. Still, just as proved true for the original cadmium(II) texaphyrin complex,[2] the reduction potentials observed for the transition-metal complexes **1**−**10** were cathodically shifted by 250−350 mV as compared to those recorded for the corresponding lanthanide(III) complexes. Additionally, while the first and second reduction potentials of the lanthanide complexes are all similar, falling between −230 and −300 mV and −720 and −760 mV (vs Ag/AgCl), respectively, those for the transition metal complexes appear to fall into two classes. The first of these consists of the Mn(II) (**1** and **8**) and Co(II) (**2**, **6**, and **9**) complexes and display first reduction potentials between −560 and −577 mV. In the second class are the Ni(II) and

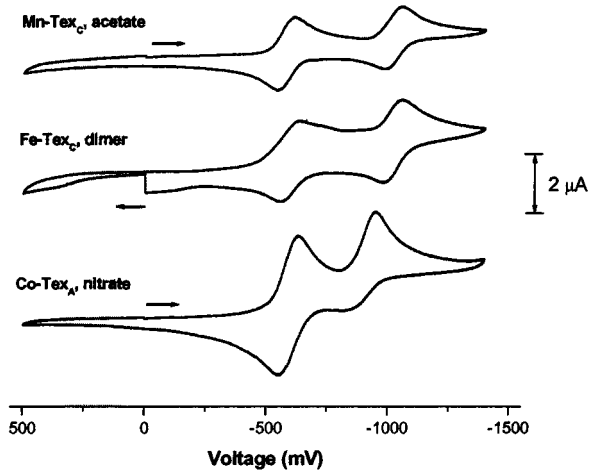

Figure 7. Cyclic voltammograms of DMSO solutions (~2×10^{-3} M) of Mn(II) texaphyrin, **8**, μ-oxo-Fe(III) dimer texaphyrin, **10**, and Co(II) texaphyrin, **2**, at 295 K. Arrows indicate the sweep direction.

(33) Pulse radiolysis studies support the notion that most redox processes involving metallotexaphyrins are ligand, as opposed to metal, centered. For instance, treatment of Gd−Tex and Lu−Tex with the pulse radiolysis-generated oxidants and reductants, hydroxyl radicals, and hydrated electrons gives rise to spectroscopic changes that are consistent only with ligand-centered oxidations and reductions, respectively. Since analogous spectroscopic changes are seen for Co−Tex under both oxidizing and reducing conditions, and Mn−Tex under reducing conditions, it is concluded that ligand-centered redox processes are dominant in these cases as well. By contrast, treating Mn−Tex with bromine radicals gives rise to changes that are best ascribed to a metal-centered oxidation process involving conversion between Mn(II) and Mn(III).

(34) Maiya, B. G.; Mallouk, T. E.; Hemmi, G.; Sessler, J. L. *Inorg. Chem.* **1990**, *29*, 3738−3745.
(35) Boucher, L. J.; Garber, H. K. *Inorg. Chem.* **1970**, *9*, 2644−2649.
(36) Tezuke, M.; Ohkatsu, Y.; Osa, T. *Bull. Chem. Soc. Jpn.* **1976**, *49*, 1435−1436.
(37) Kadish, K. M.; Sazou, D.; Liu, Y. H.; Saoiabi, A.; Ferhat, M.; Guilard, R. *Inorg. Chem.* **1988**, *27*, 1198−1204.
(38) Yamaguchi, H.; Soeta, A.; Itoh, K. *J. Electroanal. Chem.* **1983**, *159*, 347−359.

Zn(II) complexes, which show first reduction potentials in the range of −455 to −498 mV. The dimeric iron complexes are more similar to the first group, displaying E_{red} values for the first reduction event in the −561 mV to −607 mV (vs Ag/AgCl) potential range. Interestingly, a shift in the first reduction potential of ca. 95 mV was seen when the axial ligand of the cobalt complex **9** was changed from acetate to nitrate. Thus, under these latter circumstances, the cobalt texaphyrins display reduction behavior that more closely resembles that of class 2 than class 1.

The large difference between the first E_{red} of the lanthanide complexes and those of the transition-metal complexes is presumed to be a consequence of the lower charge present on the divalent metal centers of the latter group. The difference of over 100 mV that was observed within the transition-metal series, however, most likely stems from a combination of both coordination geometry and orbital (bonding) effects, as detailed in the Discussion section. That the Fe(III) dimer is reduced at the same approximate potential as the other transition metal derivatives likely reflects the covalent nature of the bonding between the metal cations and the oxygen ligand.

Discussion

Solid-state and solution-phase measurements support a division of the present transition-metal complexes of texaphyrin into two groups, consisting of Mn(II), Fe(II), Fe(III), and Co(II) complexes in one group and Ni(II) and Zn(II) derivatives in the other. This division is evidenced by breakpoints in aqueous stability, metal to nitrogen bond lengths (cf., Table 1), and reduction potentials (Table 4) and appears to coincide with the ability to achieve pentadentate coordination, for the first group, or tridentate coordination, with the latter group.

Structures of the complexes containing the larger transition-metal cations, such as Mn(II), as well as the smaller lanthanide(III) cations, such as Lu(III), represent a presumably optimal situation, where the cation is bound within the plane of the macrocycle by all five nitrogen atoms. By contrast, the smaller cations Ni(II) and Zn(II) cannot be fit well within the texaphyrin core and are coordinated by only three of its five potentially available nitrogenous donor groups. The Co(II) complexes, although involving the texaphyrin macrocycle acting as a pentadentate ligand, appear to exhibit borderline behavior. This intermediate behavior is reflected, for example, in the fact that the first reduction potential moves from −574 to −480 mV (vs Ag/AgCl) when the acetate axial ligand of complex **9** is replaced by a nitrate anion. Reduced axial ligation (i.e., as provided by nitrate relative to acetate) is expected to increase the extent of metal−macrocycle electrostatic interaction, especially in the case of the smaller metal cation, Co(II), making it easier to reduce the system in question. The aqueous stability of the Co(II) texaphyrins is also intermediate.

Perhaps the most striking feature of the texaphyrin complexes is the observation that their transition-metal cations are preferentially stabilized in a lower oxidation state compared to the corresponding porphyrin. This is not solely a consequence of ligand charge, as can be seen by comparison with the stable Co(III) oxidation state found in vitamin B_{12}, for example,[39] but is in accord with the notion that the larger texaphyrin ligand

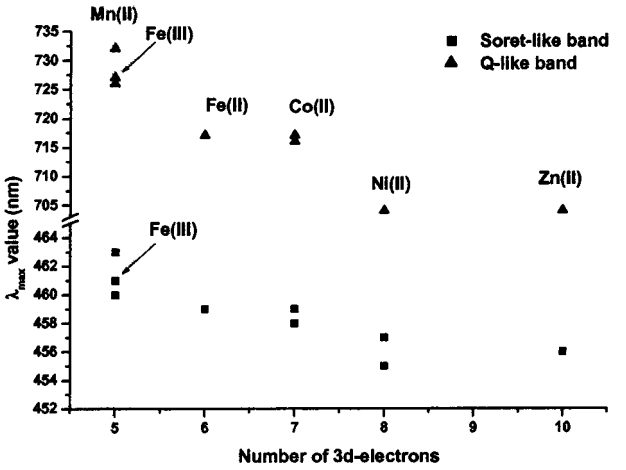

Figure 8. Plot of UV−vis absorbance maxima, λ_{max} (nm), of metallotexaphyrin complexes **1**−**10** recorded in methanol vs the number of 3d electrons on the metal cation. The concentration of the complexes was in the range of 0.1−0.3 mM.

provides a better "fit" for larger metal cations. Similarly, in contrast to porphyrins, Mn(II) is found to be the preferred oxidation state in the corresponding texaphyrin complex with the μ-oxo-dimer being the preferred form of the Fe(III) derivatives. The above, in conjunction with the high-spin metal electron configurations supported by NMR and EPR spectroscopic analyses in the case of the paramagnetic species, leads us to suggest that texaphyrin provides a weaker ligand field (and consequently less in the way of d−d orbital splitting) than does porphyrin. As is well-known, porphyrins can stabilize low-spin Co(II), Fe(II), and diamagnetic Ni(II) complexes.

The absence of a strong ligand field, however, does not appear to prevent the transition-metal cations from exerting a substantial influence on the orbital energies of the texaphyrin chromophore.[40] Indeed, the UV−vis spectra of the various transition-metal complexes feature a 23 nm blue-shift of the Q-like band as the late first-row transition-metal series is traversed from Mn(II) to Zn(II). Interestingly, similar yet much smaller blue shifts (ca. 8 nm total) were seen in the Q-like and Soret-like bands of lanthanide(III) texaphyrins, as the series was traversed from Nd(III) to Lu(III).[4] This latter finding was thought to reflect the better size complementarity and relatively improved charge neutralization associated with binding the smaller lanthanide cations.

An alternative explanation, which is not necessarily inconsistent with the above, considers the specific interactions between the metal d_{xz} and d_{yz} orbitals and the ligand π^* orbitals as a function of d electron count. Figure 8 shows a plot of the λ_{max} values for both the Soret-like and Q-like band (recorded in methanol) versus the number of 3d electrons present on the metal cation for the full set of texaphyrin complexes **1**−**10**. While subject to some scatter as the result of variations in structure, there does appear to be a general trend toward higher energy transitions as the number d-electrons increases. Possible rationales for this finding are discussed below.

If one fills in the d-orbitals in accordance with a high-spin configuration, one finds that Mn(II), like Fe(III), has 5 electrons,

(39) Halpern, J. In *B12*; Dolphin, D., Ed.; John Wiley & Sons: New York, 1982; Vol. 1, pp 501−542.

(40) DFT calculations of the relative orbital energy levels of the texaphyrin complexes **1**−**5** and their porphyrin analogues, for comparison, were performed with use of X-ray crystal structure data. Details and results of these calculations, along with orbital diagrams for each complex, can be found in the Supporting Information.

one in each d orbital, including d_{xz} and d_{yz}; Fe(II) has one paired spin in either d_{xz} or d_{yz} (all other d orbitals have one electron); Co-Tex has 2 paired spins in both d_{xz} and d_{yz}, whereas Ni(II) and Zn(II) clearly occupy a different coordination geometry. This ordering is consistent with π orbital occupancy correlating with the observed Q-band blue shift for Mn(II) ($\lambda_{max} = 732$ nm), Fe(III) ($\lambda_{max} = 732$ nm), Fe(II) ($\lambda_{max} = 717$ nm), and Co(II) ($\lambda_{max} = 713$ nm), with the 4 nm "extra" blue-shift in the Co(II) complex being due to the presence of an additional electron in the π bonding orbitals (d_{xz}, d_{yz}) as compared to Fe(II). In other words, as this portion of the transition-metal series is traversed electrons are added into metal orbitals that interact with the ligand π^* orbitals thus raising the energy of the latter. This increases the π HOMO-LUMO gap, accounting for the observed spectral changes, while making it harder to reduce the metal complexes in question.

In the case of the Ni(II) ($\lambda_{max} = 704$ nm) and Zn(II) ($\lambda_{max} = 704$ nm) complexes, both the higher nuclear charge relative to Mn(II) and Co(II) and the distinctive coordination geometry, involving only the tripyrrolydimethene, may give rise to reduced metal-to-ligand π^* orbital interactions relative to the above complexes. However, the resulting decrease in π bonding would be more than compensated for by increased σ bonding through the central pyrrole nitrogen, as evidenced by the shorter M−N bond length. In other words, if the π orbitals are lowered more than π^*, the net result would be that these complexes are relatively easy to reduce and give rise to Q-band absorptions that are comparatively blue-shifted.

Conclusions

A series of first-row transition-metal complexes of texaphyrin has been prepared and characterized. It was observed that metal cations of sufficiently high reduction potential, such as Mn(III) or Fe(III), can act to oxidize the sp^3-texaphyrin macrocycle and facilitate preparation of the corresponding complex, something not possible with lanthanide cations. While crystal structures of the largest lanthanide(III) cations, reported previously, represent one end of the coordinative limit of texaphyrin, with metal cations positioned above the plane of the pentadentate macrocycle, the solid-state structures of the complex with the smallest cation reported to date, i.e., Zn(II), represent the opposite limit of coordination, with the texaphyrin acting only as a tridentate ligand. The consequence of the expanded core of this porphyrin-like macrocycle is the stabilization of complexes with larger metal centers. This fact had already been established with the lanthanide metals, which retain their oxidation state and electron configuration in a variety of ligand environments. For transition metals, however, whose electronics are much more sensitive to ligand sphere effects, the result of this "expansion" in ligand size results in the stabilization of complexes of (generally) lower oxidation state and of higher overall spin than observed in the congeneric porphyrin systems. This salient feature coupled with the observation of new coordination modes that are readily stabilized, as seen, e.g., in the Zn(II) complex **4**, provides an incentive to explore further the coordination chemistry of texaphyrins and other expanded porphyrins.

Experimental Section

Materials. The hydrochloride salts of the so-called sp^3-form of the texaphyrin 4,5,9,24-tetraethyl-16,17-dimethoxy-10,23-dimethyl-13,20,25,26,27-pentaazapentacyclo[20.2.1.1.1.0]heptacosa-3,5,8,10,12,14(19),15,17,20,22,24-undecaene (Tex_a),[1] the 9,24-hydroxypropyl analogue (Tex_b),[1] and the water-solubilized 9,24-hydroxypropyl-16,17-di(tetraethylene-glycol) congener (Tex_c)[14] were prepared according to published procedures. All solvents, reagents, and metal salts were of reagent grade, purchased commercially, and used as such unless otherwise indicated. Methanol and dichloromethane were dried by distillation from CaH_2 when necessary. Sep-pak reverse-phase columns (C18, 10 g) were obtained from Waters, Milford, MA.

General Procedure for the Synthesis of Mn(II), Co(II), Ni(II), and Zn(II) Complexes of Tex_a (1−4). One equivalent of the sp^3-texaphyrin macrocycle was dissolved in MeOH containing ca. 10 equiv of base (triethylamine or lutidine) to give a bright red solution. Five equivalents of the metal salt were added, and the reaction mixtures were stirred for 1−24 h, protected from light, until judged complete by UV−vis spectroscopic analysis. Color change from red to green occurred in all cases. After completion, the solvent was removed under vacuum and the resulting green/blue solid dried in vacuo overnight. The complex was purified by column chromatography through silica gel with dichloromethane containing increasing amounts of methanol (10−30%) as the eluent. After the initial red/brown fraction was discarded, the green complex was generally eluted from the column with 20% MeOH/CH_2Cl_2. The product-containing fractions were washed with 2 × 50 mL of 1 M aqueous $NaNO_3$ (or NaO_2CCH_3 in the case of Mn(II) texaphyrin complex). If the complex precipitated during the wash, more methanol was added to dissolve it. The organic layer was separated, and the solvent removed under reduced pressure without heating. The complex was purified by dissolving it in a minimal amount of 30% methanol/CH_2Cl_2 and precipitated by adding this solution to ca. 200 mL of diethyl ether with rapid stirring. The resulting blue/green crystalline solid was collected and dried overnight in vacuo.

Mn(II)-Tex_a Chloride, 1: Procedure A. The sp^3-Tex_a (0.097 g, 0.164 mmol) was stirred for 1 h with ca. 0.2 mL of Et_3N and Mn(II) acetate tetrahydrate (0.125 g, 0.510 mmol). After the general workup procedure described above was employed, without the exchange of the counteranion, 0.078 g (72%) of the complex was isolated. Crystals suitable for X-ray diffraction were obtained by dissolving the complex in a minimal amount of 20% MeOH/CH_2Cl_2 (structure **1**) or MeOH (structure **1**$(MeOH)_2Cl$) and inducing crystallization by vapor diffusion of Et_2O. Analytical data are presented following the summary of procedure B below.

Mn(II)-Tex_a Acetate, 1: Procedure B. The sp^3-Tex_a (0.075 g, 0.127 mmol) was stirred for 1 h with 0.15 mL of Et_3N and Mn(III) acetate dihydrate (0.147 g, 0.633 mmol) in 50 mL of methanol. After workup with the general procedure described above, 0.060 g (71%) of the product was obtained. UV−vis (MeOH) [λ_{max}, (log ϵ)]: 406 (4.55), 460 (4.96), 727 (4.51). UV−Vis(CH_2Cl_2) [λ_{max}, (log ϵ)]: 464 (4.43), 734 (4.09). MS(FAB), M^+: 603. Anal. Calcd for [$C_{36}H_{41}N_5O_4Mn \cdot 1.5H_2O$]: C, 62.69; H, 6.43; N, 10.15. Found: C, 62.54; H, 6.22; N, 10.02.

Co(II)-Tex_a Nitrate, 2. 2 was obtained in 60% yield by using the general procedure described above. Crystals suitable for X-ray diffraction were obtained by vapor diffusion of Et_2O into a concentrated solution of the product in 20% MeOH/CH_2Cl_2. UV−vis (MeOH) [λ_{max}, (log ϵ)]: 406 (4.49), 457 (4.75), 713 (4.21). MS(FAB), M^+: 607. Anal. Calcd for [$C_{34}H_{38}N_6O_5Co \cdot CH_2Cl_2$]: C, 55.71; H, 5.34; N, 11.14. Found: C, 54.94; H, 5.77; N, 11.75.

Ni(II)-Tex_a Nitrate, 3. 3 was obtained in 40% yield by using the general procedure described above. UV−vis (MeOH) [λ_{max}, (log ϵ)]: 399 (4.68), 457 (4.98), 704 (4.56). MS(CI), M^+: 608. Anal. Calcd for [$C_{34}H_{38}N_6O_5Ni \cdot 1.5CH_2Cl_2 \cdot CH_3OH$]: C, 53.20; H, 5.33; N, 10.34. Found: C, 52.01; H, 5.31; N, 11.35.

Zn(II)-Tex_a Nitrate, 4. 4 was obtained in 65% yield by using the general procedure described above. Crystals suitable for X-ray diffraction were obtained by slow diffusion of Et_2O into a concentrated 10% MeOH/CH_2Cl_2 solution (structure **4**) or in a concentrated methanol solution (structure **4**$(MeOH)_2NO_3$) of the product, each containing one

drop of Et_3N. ^1H NMR (CD_3OD): δ 1.76 (t, 6H, CH_2CH_3), 1.77 (t, 6H, CH_2CH_3), 3.39 [s, 6H, pyrr-CH_3], 3.80 [d(q), 8H, CH_2CH_3], 4.50 [s, 6H, Ph-OCH_3], 9.37 [s, 2H, Ph-H], 9.74 [s, 2H, $(pyrr)_2$-CH], 11.96 [s, 2H, H-C=N]. ^{13}C NMR (CD_3OD): δ 10.4, 18.1, 18.9, 20.0, 20.1, 57.43, 99.5, 114.1, 135.11, 139.2, 145.8, 147.4, 150.8, 151.5, 154.8, 157.6. UV−vis (MeOH) [λ_{max}, (log ϵ)]: 399 (4.41), 456 (4.77), 704 (4.30). MS(FAB), M^+: 612. Anal. Calcd for [$C_{34}H_{38}N_6O_5Zn\cdot CH_2Cl_2\cdot 2CH_3OH$]: C, 53.86; H, 5.86; N, 10.19. Found: C, 53.33; H, 5.17; N, 10.78.

Synthesis of Bis-μ-oxo-Fe(III)-Tex$_a$ Dinitrate, 5. The sp^3-Tex$_a$ (0.075 g, 0.127 mmol) was stirred with 0.15 mL of lutidine and Fe(III) nitrate nonahydrate (0.257 g, 0.636 mmol) in 50 mL of methanol. The reaction mixture was heated to reflux temperature while stirring open to the air for ca. 5 h. After cooling, all solvents were removed under reduced pressure. The resulting green/brown solids were dissolved in a minimal amount of 1% methanol/CH_2Cl_2 and added to a column of neutral alumina prepared with the same solvent mixture. The polarity of the eluent was slowly increased to first a mixture of 2% and then 5% methanol in CH_2Cl_2 until the gold/brown product was eluted. Product fractions were collected, all solvents were removed with a rotary evaporator, and the solid was dried under vacuum. The product was recrystallized by dissolving in a minimal amount of CH_2Cl_2 and precipitating with hexanes. The resulting brown/green solid was collected and dried in vacuo to yield 0.040 g of product (51%). Crystals of the complex suitable for X-ray diffraction were obtained by slow diffusion of Et_2O into a methanol solution of the product. UV−vis (MeOH) [λ_{max}, (log ϵ)]: 409 (4.65), 458 (4.72), 732 (4.24). MS(FAB), M^+: *m/e* 610 (for $[C_{68}H_{76}N_{10}Fe_2O]^{2+}$). Anal. Calcd for [$C_{68}H_{76}N_{10}O_5Fe_2Cl_2\cdot CH_2Cl_2$]: C, 60.01; H, 5.69; N, 10.14. Found: C, 60.64; H, 5.87; N, 10.32.

Complexes with Tex$_b$ and Tex$_c$ ligands are much more hydrophilic than those of Tex$_a$. Therefore, while synthetic methods are nearly identical, alternative means were used for optimal purification of complexes **6**−**10**. These methods are described in detail in the Supporting Information.

Synthesis of Co(II)-Tex$_b$ Acetate, 6. The hydrochloride salt of sp^3-Tex$_b$ (0.80 g, 1.23 mmol) was dissolved in 200 mL of methanol. A 50 mL methanolic solution of cobaltous acetate tetrahydrate (487 mg, 1.95 mmol) was added to the texaphyrin solution, followed by triethylamine (1.8 mL, 1.3 mmol). After 30 min, the solvents were removed under reduced pressure and the residue dried under high vacuum. Purification of this compound was achieved by re-extraction and precipitation to give 0.521 g of pure complex (55%). UV−vis (CH_3OH) [λ_{max}, (log ϵ)]: 341 (4.69), 459 (4.80), 716 (4.28). MS(FAB), M^+: 667.0. Anal. Calcd for [$C_{38}H_{49}N_5O_8Co$]: C, 59.84; H, 6.48; N, 9.18; Co, 7.73. Found: C, 59.41; H, 6.47; N, 9.23; Co, 6.97. Magnetic moment (Evans): 4.19 μ_B

Synthesis of Ni(II)-Tex$_b$ Nitrate, 7. The hydrochloride salt of the sp^3-Tex$_b$ (0.077 g, 0.118 mmol) was stirred with 0.13 mL of lutidine and Ni(II) nitrate hexahydrate (0.172 g, 0.592 mmol) in 150 mL of methanol, open to air but protected from light, for 24 h. Solvent was removed under reduced pressure. Purificationn was achieved through column chromatography and precipitation. The green solid was collected on and dried overnight in vacuo to yield 0.053 g of product (66%). UV−vis (MeOH) [λ_{max}, (log ϵ)]: 399 (4.69), 455 (4.92), 705 (4.53). Calcd for [$C_{36}H_{42}N_6O_7Ni\cdot CH_2Cl_2$]: C, 54.57; H, 5.45; N, 10.32. Found: C, 54.06; H, 5.84; N, 11.16.

Synthesis of Mn(II)-Tex$_c$ Acetate, 8. The hydrochloride salt of sp^3-Tex$_c$ (1.00 g, 1.08 mmol), manganese acetate tetrahydrate (323 mg, 1.30 mmol), triethylamine (1.51 mL, 10.8 mmol), and methanol (250 mL) were stirred at ambient temperature, open to the atmosphere, for 30 min. The solvents were then removed under reduced pressure, and the residue was dried overnight under high vacuum. Purification was achieved by Sep-pak chromatography and precipitation to yield 718 mg (67%) of dark green powder. UV−vis (DMSO) [λ_{max}, nm (log ϵ)]: 468 (4.91), 731 (4.42). Positive ESI-MS (methanol), M^+: 931. Anal. Calcd for [$C_{50}H_{69}N_5O_{12}Mn$]: C, 60.84: H, 7.05; N, 7.10; Mn, 5.57. Found: C, 60.17; H, 7.23; N, 7.08; Mn, 5.16. Magnetic moment (Evans): 5.91 μ_B

Synthesis of Co(II)-Tex$_c$ Acetate, 9. The hydrochloride salt of sp^3-Tex$_c$ (1.00 g, 1.08 mmol), cobaltous acetate tetrahydrate (323 mg, 1.30 mmol), triethylamine (1.51 mL, 10.8 mmol), and methanol (250 mL) were combined and stirred at ambient temperature open to the atmosphere for 30 min. The solvents were removed under reduced pressure, and the residue was dried under high vacuum overnight. Purification was conducted by using the same procedure as for compound, **8**. This gave **9** as a green powder (718 mg, 67%). UV−vis (CH_3OH) [λ_{max}, nm (log ϵ)]: 340 (4.38), 406 (4.58), 458 (4.83), 672 (3.97), 716 (4.29). Positive ESI-MS (methanol), M^+: 931. Anal. Calcd for [$C_{50}H_{69}N_5O_{12}Co\cdot H_2O$]: C, 59.52; H, 7.09; N, 6.94; Co, 5.84. Found: C, 59.3; H, 7.20; N, 7.23; Co 4.49. Magnetic moment (Evans): 4.22 μ_B.

Synthesis of Bis-μ-oxo-Fe(III)-Tex$_c$ 10. The hydrochloride salt of sp^3-Tex$_c$ (2.00 g, 2.16 mmol), ferrous acetate (452 mg, 2.60 mmol), triethylamine (3.02 mL, 21.6 mmol), and methanol (500 mL) were combined. The solution was heated at reflux open to the atmosphere for 10 h. After allowing the mixture to cool with stirring overnight, a UV−vis spectrum indicated absorbances at 408, 456, and 734 nm. Solvents were removed under reduced pressure, and the residue was dried under high vacuum overnight. Purification was performed with Sep-pak chromatography and precipitation to provide **10** as a brown/green powder (1.145 g, 53%). UV−vis (CH_3OH) [λ_{max}, nm (log ϵ)]: 224 (4.63), 268 (4.62), 342 (4.76), 408 (4.90), 450 (4.88), 732 (4.34). Positive ESI-MS (methanol), M^+: *m/e* 937 (calcd for $[C_{96}H_{132}N_{10}O_{21}Fe_2O]^{2+}$). Magnetic moment (Evans): 6.01 μ_B (per molecule of dimer). Anal. Calcd for [$C_{100}H_{138}Fe_2N_{10}O_{25}\cdot 2H_2O$]: C, 59.23; H, 7.06; O, 21.30; Fe, 5.51. Found: C, 58.87; H, 6.87; N, 6.84; Fe, 5.22.

Magnetic Moment. Experiments were performed with the Evans method.[24] The texaphyrin complex (0.50−2.00 mg) was dissolved in 0.65−0.9 mL of CD_3OD. Pure CD_3OD was placed in a concentric tube within the NMR tube. Measurements, made in duplicate, were performed with either a 300 MHz Varian Unity or a QE 300 NMR spectrometer. Calculations of magnetic moments were based on the difference in chemical shift observed for the residual methyl group signal in neat solvent and in paramagnetic solution.

Electrochemistry. Electrochemical measurements were carried out at ambient temperature with a Cypress System 1090 apparatus in cyclic voltammetry mode. All reported electrochemical half-wave potentials were measured with use of a Ag/AgCl reference electrode and a glassy carbon working electrode. Platinum wire (0.5 mm diameter) was employed as an auxiliary electrode. Each experiment was performed on a 1−3 mM solution of texaphyrin complex in 1 mL of DMSO, using 0.1 M tetrabutylammonium perchlorate as the supporting electrolyte.

The potential was scanned between +1200 and −2000 mV. The ferrocene/ferrocenium redox couple was observed at +476 ± 3 mV in this electrochemical setup. Peak potentials were found to be insensitive to scan rate in the range 500−50 mV/s. The electrochemical potentials presented in this paper were obtained at 50 mV/s. The scan direction was changed for each complex studied to determine the reversibility of observed redox processes. Reduction potentials reported for metallotexaphyrins are presented as the average value of triplicate measurements with error expressed as the standard deviation.

Photophysical Measurements. Emission spectra, fluorescence spectra, laser flash photolysis, and singlet oxygen quantum yields experiments were performed as described in ref 4.

X-ray Crystallography. Deep-blue platelike crystals of **1**, **1**$(MeOH)_2Cl$, **2**$(MeOH)_2Cl$, **4**, **4**$(MeOH)_2NO_3$, and **5**, stabilized in mineral oil were mounted on a glass fiber at room temperature then quickly cooled to 150 or 123 K with an Oxford Cryostream low-temperature device. Preliminary examination and data collection were performed on a Nonius Kappa CCD diffractometer with a graphite monochromator

Table 5. Crystallographic Data for Complexes **1**$(MeOH)_2Cl$, **2**, **4**, **4**$(MeOH)_2NO_3$, and **5**

	1$(MeOH)_2(Cl)$	**2**$(MeOH)_2Cl$	4	**4**$(MeOH)_2NO_3$	5
formula	$C_{37}H_{50}N_5O_5ClMn$	$C_{37}H_{50}N_5O_5ClCo$	$C_{35}H_{40}Cl_{2.60}N_{5.40}O_{3.20}Zn$	$C_{37}H_{50}N_6O_8Zn$	$C_{79}H_{108}N_{12}O_{19}Fe_2$
formula wt	735.21	739.20	745.06	772.20	1592.62
crystal system	monoclinic	monoclinic	monoclinic	triclinic	orthorhombic
space group	$P2_1/n$	$P2_1/n$	$P2_1/c$	$P\bar{1}$	*Pbcn*
color of crystal	deep blue	deep blue	deep blue	deep blue	deep blue
a, Å	10.3820(5)	10.313(2)	12.7413(9)	10.1139(3)	20.887(4)
b, Å	34.7520(13)	34.772(7)	21.9120(10)	12.2184(3)	22.044(4)
c, Å	10.6580(5)	10.656(2)	12.8959(9)	17.0673(5)	18.080(4)
α, deg				93.298(2)	90
β, deg	100.332(2)	100.80(3)	105.626(4)	104.553(1)	90
γ, deg				113.643(2)	90
V (Å^3), Z	3783.0(3), 4	3753.6(13), 4	3467.3(4), 4	1840.03(9), 2	8325(3), 4
d(calcd), g/cm^3	1.29	1.308	1.427	1.394	1.271
absorp coeff (mm^{-1})	0.467	0.576	0.953	0.728	0.419
no. of frames of data	307	194	447	487	109
scan range (ω scans) (deg)	1	1.9	1	0.9	1.9
time/frame, (s)	189	741	286	90	114
total no. of reflcns	25440	10896	11215	12316	10328
no. of unique reflcns	8617	7395	6138	7998	10328
no. of obsd reflcns [$I > 2\sigma(I)$]	4590	4063	3780	6270	6634
T, K	123(2)	123(2)	153(2)	153(2)	153(2)
R,[a] R_w[a] (%)	6.50, 14.2	13.2, 22.0	11.3, 17.8	4.65, 6.84	6.09, 10.3

[a] $R = \sum||F_o| - |F_c||/\sum F_o$ for reflections with $F_o > 4(\sigma(F_o))$. $R_w = \{[\sum w(F_o^2 - F_c^2)^2]/[\sum w(F_o^2)^2]\}^{1/2}$.

with Mo Kα radiation ($\lambda = 0.71073$ Å). Details of crystal data, data collections, and structure refinement are given in Table 5. Data reduction was performed with DENZO-SMN.[41] The structures were solved by direct methods with SIR92[42] and refined by full-matrix least-squares on F^2 with anisotropic displacement parameters for the non-H atoms with SHELXL-97.[43] The hydrogen atoms on carbon were calculated in ideal positions with isotropic displacement parameters set to 1.2 × U_{eq} of the attached atom (1.5 × U_{eq} for methyl hydrogen atoms). Neutral atom scattering factors and values used to calculate the linear absorption coefficient are from the International Tables for X-ray Crystallography.[44] All figures were generated with SHELXTL/PC.[45]

For **2**$(MeOH)_2Cl$, difficulty in refinement occurred. Details of the refinement of this structure, including confirmation of the presence of a mixture of two anions, nitrate and chloride, are located in the Supporting Information. Further crystallographic details for all complexes, including tables of positional and thermal parameters, bond lengths and angles, figures, and lists of observed and calculated structure factors, are also found in the Supporting Information.

Acknowledgment. This work was supported in part by the NIH (Grant No. CA 68682 to J.L.S. and Grant No. GM 19547-01 to S.H.) and the Office of Basic Energy Sciences of the U.S. Department of Energy. This is document NDRL-4377 from the Notre Dame Radiation Laboratory. We also thank Professor Paul Lindahl and Huey King Loke at Texas A&M University for recording the EPR spectra.

Supporting Information Available: Additional data from UV−vis, decomposition experiments, EPR, photophysical measurements, electrochemistry, and DFT calculations, as well as crystallographic details (PDF). This material is available free of charge via the Internet at http://pubs.acs.org..

JA012747A

(41) Otwinowski, Z.; Minor, W. *Methods Enzymol. Part A* **1997**, *276*, 307−326.
(42) Altomare, A.; Cascarano, G.; Giacovazzo, C.; Guagliardi, A. *J. Appl. Crystallogr.* **1993**, *26*, 343−350.
(43) Sheldrick, G. M. *SHELXL97*, Program for the Refinement of Crystal Structures; University of Gottingen: Germany, 1994.
(44) *International Tables for X-ray Crystallography*; Wilson, J. C., Ed.; Kluwer Academic Press: Boston, 1992; Vol. C, Tables 4.2.6.8 and 6.1.1.4.
(45) Sheldrick, G. M. *SHELXTL/PC*, Version 5.03; Siemens Analytical X-ray Instruments, Inc.: Madison, WI, 1994.